Journal of Alloys and Compounds, 610 (2014) 92-99
http://dx.doi.org/10.1016/j.jallcom.2014.04.195

Extracting the composition of nanocrystals of mechanically alloyed systems using Mössbauer spectroscopy

J. S. Blázquez, J. J. Ipus, V. Franco, C. F. Conde, A. Conde

Departamento de Física de la Materia Condensada, Universidad de Sevilla, P.O. Box 1065, 41080, Sevilla, Spain

Abstract

Determining the composition at the nanoscale generally requires the use of experimental techniques such as 3D atom probe or nanoanalysis, which have limited availability, involve high economic cost and, moreover, imply aggressive sample preparations. However, the combination of Mössbauer spectrometry (MS), X-ray diffraction (XRD) and magnetization measurements can supply very detailed information on the average values of composition of tiny elements of the microstructure such as nanocrystals and boundary regions. Unlike nanoscale techniques, those techniques are widely accessible to most of the scientific community and do not require any special sample preparation, especially for powder samples. Two methods are proposed: the first method uses the ratio between the high field contributions to the MS spectra to extract the composition of the nanocrystals and allows us to follow its evolution; the second method uses average values of the hyperfine field and XRD data to study nanocrystalline samples. These procedures have been applied to two FeNb(B) powder samples obtained by mechanical other isotopes suitable for Mössbauer spectroscopy or to data from nuclear magnetic resonance experiments.

Journal of Alloys and Compounds, 610 (2014) 92-99
http://dx.doi.org/10.1016/j.jallcom.2014.04.195

1 Introduction

Compositional and microstructural characterization of materials is a key point to optimize technological properties, to understand the underlying physics and to develop theories and models to go further in Materials Science. This characterization is especially tricky for nanoscale systems, for which the characteristic size to be analyzed can be so small that could apparently be only accessible to nanoprobe techniques (such as high resolution transmission electron microscopy, 3D atom probe, atomic force microscopy, etc.). The presence of irregularities even at such scales implies non simple interpretation of the results. In addition, nanoscale techniques, in general, require costly (economically and in time) sample preparation procedures and limit the explored region to a very small part of the sample (where, artifacts due to the effects of sample preparation might also play a role). Therefore, a very detailed but local information is obtained and it must be extrapolated to the overall system. Unlike these techniques, conventional ones such as X-ray diffraction or Mössbauer spectroscopy can supply average information of a sample with a macroscopic size. These techniques are widely used to identify the phases present in the material and some other structural characteristics such as crystal size, microstrains, lattice parameter, etc. In fact, compositional information can be derived from Mössbauer data but requires further analysis in combination with other experimental techniques. In fact, the capabilities of Mössbauer spectroscopy to analyze nanoscale systems have been pointed out by different authors [1,2,3,4].

For magnetic applications, the reduction of the characteristic microstructural length to nanometer scale leads to outstanding properties. In fact, nanocrystalline microstructures are common to both the hardest [5,6] and the softest magnetic materials known [7]. In this sense, ball milling techniques have been proved as a very efficient tool to obtain metastable systems such as nanocrystalline and amorphous materials [8]. In particular, it is remarkable the synthesis of permanent magnets, especially modern rare earth lean/free ones [9,10,11,12] and the production of amorphous/nanocrystalline soft magnetic materials [13].

Journal of Alloys and Compounds, 610 (2014) 92-99
http://dx.doi.org/10.1016/j.jallcom.2014.04.195

Mechanical alloying is a particular case of ball milling technique, which was first developed by Benjamin [14]. The starting material for this technique, which is compositionally heterogeneous (generally pure elements), becomes homogenized after milling forming an alloy. Therefore, the compositional evolution of the different phases is particularly interesting for samples produced using this technique in order to determine the time needed to get an optimally homogenized sample. ^{57}Fe Mössbauer spectroscopy has been frequently used to follow the compositional evolution of the Fe containing phases present in the mechanically alloyed powders. However, generally only a qualitative description is given based on the evolution of the average hyperfine field corresponding to a particular phase (e.g. ref. [15,16,17]). Pandey et al. [18] performed a quantitative analysis using a binomial distribution considering the two first shells of Fe to describe the mechanical alloying of Fe-Cr binary alloys. However, they assigned the reduction of the relative area of the contribution at 33 T to compositional effects although they pointed out the possible effects of other factors as defects. In the present work, we propose a procedure to afford a quantitative analysis of the composition evolution of mechanically alloyed powders taking into account the crystal size effects and the presence of an interface region, which contribution to the Mössbauer spectra differs from that of the core.

In this work, the composition of nanocrystals of bcc Fe-based supersaturated solution obtained by mechanical alloying Fe-Nb-(B) powders is obtained through a systematic analysis of the Mössbauer data and their relationship with microstructural and magnetic parameters. The chosen compositions are $Fe_{85}Nb_5B_{10}$ and $Fe_{94.4}Nb_{5.6}$ (with the same Fe/Nb ratio). Both compositions develop a supersaturated solid solution with a microstructure formed by nanocrystals (see TEM images in [19]). We avoid compositions with a lower Fe content, which lead to the formation of amorphous phases [19,20], where a description by a binomial distribution in terms of the first and second shells surrounding a Fe atom is not appropriate. We propose two different methods to determine the composition of nanocrystalline structures. The first method uses the ratio between the two higher field contributions to the Mössbauer (MS) spectra (less affected by microstructure) to extract the average composition of the core of the

Journal of Alloys and Compounds, 610 (2014) 92-99
http://dx.doi.org/10.1016/j.jallcom.2014.04.195

nanocrystals and allows us to determine its compositional evolution; the second method uses average values of the hyperfine field combined with microstructural data obtained from X-ray diffraction (XRD) to study nanocrystalline samples. A good agreement is found between both methods.

The procedures developed in this paper do not require the use of nanoscale techniques (e.g. atom-probe, high resolution electron microscopy, etc.) and can be easily extended to other nanocrystalline materials of interest, including systems containing other isotopes suitable for Mössbauer spectroscopy [21] or using nuclear magnetic resonance experiments [22].

2 Experimental

Thirty grams of pure element powder mixtures of nominal compositions $Fe_{94.4}Nb_{5.6}$ and $Fe_{90}Nb_5B_{10}$ (both with the same Fe/Nb ratio) were ball milled using steel balls and hardened steel vials in a Fritsch Pulverisette Vario 4 planetary mill. Milling parameters were: 350 rpm for the frequency of the main disk and -700 rpm for the frequency of the vials, ball to powder ratio was 10:1 in 250 cm^3 vials with 75 balls of 10 mm diameter. Milling was performed in argon atmosphere and all the manipulation of the powders was done under protective argon atmosphere in a Saffron Omega glove box with oxygen and humidity levels below 1 ppm.

XRD experiments were performed in a Bruker D8 I diffractometer using Cu-Kα radiation. The acquired patterns were fitted using TOPAS software and Pawley method [23] (full pattern fitting) in order to obtain the crystal size and microstrains of the phases. To do so, microstrains and crystal size effects were considered to yield Gaussian and Lorentzian profiles, respectively, of the diffraction maxima.

Scanning electron microscopy (SEM) experiments were performed in a Jeol 6460 LV microscope operated at 20 kV. Images in back scattered electrons (BSE) mode in combination with energy dispersive spectroscopy (EDS) were used to identify compositional distribution.

Journal of Alloys and Compounds, 610 (2014) 92-99
http://dx.doi.org/10.1016/j.jallcom.2014.04.195

For Fe containing systems, ^{57}Fe Mössbauer spectrometry is a very powerful technique to obtain information of the Fe containing phases in the sample and to correlate microstructural and magnetic results [21]. Mössbauer spectrometry (MS) experiments in a transmission geometry were performed using a ^{57}Co(Rh) source. Values of the hyperfine parameters (isomer shift, *IS*, quadrupole splitting, *Q*, and the hyperfine field, *HF*) were obtained by fitting with NORMOS program [24]. The isomer shift, *IS*, was quoted relative to the Mössbauer spectrum of an α-Fe foil at room temperature.

Magnetization curves were recorded at room temperature using a Lakeshore 7407 vibrating sample magnetometer (VSM) with a maximum applied magnetic field $\mu_0 H$=1.5 T. Spontaneous specific magnetization, σ_S, was obtained from the extrapolation of high field $\sigma(B)$ curve to zero field.

3 Results

3.1 XRD results

Figure 1 shows the evolution of the XRD patterns of the different alloys as a function of milling time. Patterns have been normalized to the area of the (110) maxima of bcc Fe. The bcc Fe diffraction maxima get broader as milling time increases due to the progressive increase of microstrains and the reduction of crystal size. Moreover, a shift to lower angles of bcc Fe maxima evidences an increase of the lattice parameter as Nb atoms become incorporated into the bcc Fe(Nb) supersaturated solid solution (B atoms in bcc Fe should lead to a reduction of the lattice parameter [25] and this effect is hidden by the stronger effect of Nb). Peaks ascribed to bcc Nb phase are only detected for short milling times (t<2 h), indicating that this phase disappears as the Nb atoms become dissolved in the bcc Fe matrix. No amorphous phase was detected. Figure 2 shows the main results obtained from the XRD patterns corresponding to bcc Fe phase: microstrains (ε), crystal size (D) and lattice parameter (a) as a function of milling time. Whereas no sifgnificant difference is found with B addition for microstrains and lattice

Journal of Alloys and Compounds, 610 (2014) 92-99
http://dx.doi.org/10.1016/j.jallcom.2014.04.195

parameter, crystal size is clearly larger for the B-free alloy, for which a stable value ~30 nm is rapidly achieved. For the B-containing alloy, *D* continuously decreases down to ~5 nm. Therefore, it is inferred that B plays an important role in reducing the crystal size: hard boron inclusions should act as an extra milling media in the B-containing alloy. Very similar results were obtained using crystalline boron instead of amorphous boron in the starting mixture [26,27].

3.2 Scanning electron microscopy results

Figure 3 shows back scattered electron (BSE) images for B-containing samples milled 0.5 h. As observed, large bright zones with irregular shape corresponding to Nb rich regions are clearly identified, mixed with a darker majority region corresponding to Fe rich zones. In addition, small dark spots (~250 nm) which correspond to boron particles can be observed at a higher magnification. EDS analysis confirms this compositional identification inferred from BSE images. Further milling leads to the disappearance of the bright Nb regions, indicating the homogenization of Fe and Nb at the explored scale. However, boron inclusions remain, without appreciable change in their size after 6 h of milling but reducing to ~100 nm after 40 h of milling. Using Kanaya-Okayama formula [28,29], the maximum penetration depth, *R*, of the electrons in a solid can be calculated as:

$$R = \frac{bAV_0^{5/3}}{\rho Z^{8/9}} \quad (1)$$

where A is the atomic mass, V_0 is the accelerating voltage, ρ is the density and Z the atomic number. The prefactor b is 0.0277 μm·mol·cm^{-3}kV^{-1}, and thus R is obtained directly in μm when units of A, V_0 and ρ are g/mol, kV and g/cm^3, respectively. For iron, this depth is ~1.5 μm, one order of magnitude larger than the size of the observed boron inclusions, which could explain the weaker contrast between the matrix and the inclusions as they become smaller.

Journal of Alloys and Compounds, 610 (2014) 92-99
http://dx.doi.org/10.1016/j.jallcom.2014.04.195

Boron inclusions have been observed by transmission electron microscopy in similar Fe-Nb-B systems [27,19,30] and other alloys [31,32] which implies that an important amount of this element remains unalloyed and that boron content in the matrix must be lower than the nominal composition.

3.3 Mössbauer spectroscopy results

Figure 4 shows the evolution of the Mössbauer spectra with milling time. It can be observed that the sextet ascribed to the α-Fe type phase continuously broadens as milling time increases due to the progressive formation of the supersaturated bcc Fe(Nb,B) solid solution and to a reduction of the crystal size, as will be described below. Fitting of complex spectra as those studied here is not free from ambiguities [3,33]. Theoretically, each kind of Fe environment should provide a characteristic sextet (for ferromagnetic sites), doublet (for paramagnetic sites with significant quadrupolar splitting) or singlet (for paramagnetic sites with negligible quadrupolar splitting). In the present case, a supersaturated solid solution with up to three possible elements leads to numerous different Fe environments. Moreover, the very small size of the crystallites leads to a non-negligible amount of atoms in the surface of the crystals, which are affected by the surrounding region outside the crystal (e.g. crystalline boundaries), enriched in those elements for which the crystals are depleted. This contribution corresponds to the so-called interface region [1,2]. The Fe atoms located in this region have a reduced hyperfine field with respect to those atoms located in the core of the crystal. In addition, it must be taken into account that, for bcc structures, the ratio between the distances of near neighbors (NN) and next near neighbors (NNN) to the probe Fe is only 0.87 indicating that the effect of the second shell in the central Fe probe is not negligible.

Therefore, in order to simplify fitting of the obtained spectra, hyperfine field distributions (*HFDs*) are generally used with a linear relationship between *HF* and *IS* [21]. We have used two different *HFDs* to fit the experimental Mössbauer spectra: one for low *HF* values (from 0 to 14 T) and another for high *HF* values (from 8 to 39 T). The reason for using two

HFDs is the different nature expected for low *HF* contributions (Fe atoms in Nb/B rich environments; e.g. as impurities in Nb crystals or B inclusions, or at the grain boundaries) and high *HF* contributions (Fe atoms in bcc crystals). In order to apply the same criteria, these two *HFDs* have been used for all the studied milling times. This decision implies two possible artifacts to be considered: paramagnetic contributions, which should correspond to *HF*=0, could also be fitted using very low *HF* (<5 T); and some artificial contributions can arise when inner lines of a high *HF* contribution are erroneously considered as external lines of a lower *HF* contribution. These problems are enhanced by the presence of the interface regions. In the following discussion, these problems will be overcome after considering contributions below 5 T as paramagnetic and mainly concentrating the analysis to high *HF* contributions, i.e. those less affected by the drawbacks described above. Figure 5 shows some examples of the *HFD*s obtained. It is worth mentioning that each of the two *HFD*s used to fit the spectra do not have a one to one correspondence to each particular region considered in the physical description of the samples (core of nanocrystals and interface), but this fitting model allows us to obtain an experimental distribution of *HF*. This phenomenological hyperfine field distribution will be described as a sum of Gaussian functions which should correspond to different Fe environments. The contribution from the interface region (with lower *HF* values) might not overlap with the highest *HF* values and, therefore, these contributions can be assigned to pure Fe environments at the core region.

Figure 6a-c shows the fraction of Fe atoms contributing with *HF*<5 T, the average values of hyperfine magnetic field (<*HF*>), and of the isomer shift (<*IS*>) as a function of milling time for both studied alloys. Values of <*IS*> show a common behavior for the two alloys, indicating that this parameter is mainly affected by Nb and not by B (or that B content in the bcc supersaturated solid solution is very low). Initially, for short milling times (t~1.5-2 h), for which bcc Nb phase is detected by XRD, a strong reduction of <*IS*> is observed and, after further milling, <*IS*> increases and reaches a stable and positive value. The large error bars of this parameter (±0.01 mm/s) prevent further discussion about it.

Journal of Alloys and Compounds, 610 (2014) 92-99
http://dx.doi.org/10.1016/j.jallcom.2014.04.195

Unlike <*IS*>, the behavior of <*HF*> as milling time increases depends on the alloy. Although the trend is common for both studied alloys below 3.5 h milling, a clear minimum is only observed for the B-free alloy after 3.5 h milling. For the B-containing alloy, <*HF*> continuously decreases due to the effect of boron incorporation into the matrix and/or to the continuous decrease of the crystal size, as will be discussed below.

3.4 Magnetization results

Spontaneous specific magnetization, σ_S, measured as the extrapolation to zero field of the high field magnetization is shown in figure 6d. This magnitude shows a similar trend than that observed for <*HF*>. Whereas the B-containing alloy exhibits a continuous decrease in σ_S as milling time increases, for the B-free alloy this magnitude initially decreases to achieve an almost constant value for milling times above 6 h. Magnetization curves at room temperature are shown in figure 7.

4 Discussion

4.1 Composition of the core of nanocrystals

The *HFD* contributions at very low *HF* (<5 T) shown in figure 6a describe a similar trend for both studied alloys with a clear maximum at 2.5 h milling and a rapid reduction after 6 h to an almost constant value, clearly lower for the B-free alloy. This maximum must be ascribed to Fe atoms surrounded by a high number of Nb atoms. At this milling stage, where Nb crystals are still detected by X-ray, a possible contribution should be Fe atoms dissolved in these Nb crystals. However, another contribution can be understood considering the deformation of the ductile Nb crystals before Nb atoms become completely dissolved in bcc Fe matrix. Figure 8 is a simple cartoon illustrating this process for a 2D frame. At very early stages of milling, Nb crystals are not strongly deformed and are clearly detected in XRD patterns. At milling times corresponding to the maximum value observed for *HF*<5 T contribution, Nb

crystals are strongly deformed and elongated (in agreement with the EDS maps [19]), increasing their surface area and thus the number of Fe atoms facing these surfaces, with a large number of Nb neighbors also increases. Therefore, this maximum in *HF*<5 T contribution coexists with a high fraction of unaffected Fe environments (those located far enough from Nb crystals). At this stage diffraction maxima of bcc Nb phase become undetectable. After longer milling times, Nb atoms become dissolved into the matrix and thus the fraction of unaffected Fe environments is reduced, making large concentrations of Nb atoms surrounding Fe highly improbable. Values of <*IS*> also exhibit a minimum at ~2 h, which should be related to this process. Fe impurities on bcc-Nb give place to other possible Nb rich environments registered in *HF*<5 T contribution. In fact, *IS* for Fe into bcc-Nb is -0.02 mm/s and being more negative as pressure increases [34].

For binary Fe-Nb alloys, literature data [35] show that the *HF* of Fe is affected by the presence of Nb as NN (ΔHF=-3.55±0.15 T per Nb atom) or NNN (ΔHF=-2.30±0.24 T per Nb atom). Taking into account both shells, the expected values of *HF* could be obtained by averaging the Nb effect as NN and NNN, resulting in an average ΔHF=-3.0±0.2 T per Nb atom as NN or NNN, which corresponds to a low Nb content in α-Fe. Nevertheless, the effect of a larger Nb content in the environment formed by the 14 atoms (8 NN and 6 NNN) surrounding the Fe probe deviates from linearity, as it is generally found for other non-magnetic elements substituted for Fe [36,37,38]. Therefore, several Gaussian functions were used to fit the high field region of the *HFD*s (see figure 5). The Gaussian functions used to fit the broad peak observed in the distributions were centered at 33, 30 and 27 T for n=0, 1 and 2, respectively, being n the number of Nb atoms as NN or NNN. The effect of the interface regions is to reduce *HF* with respect to the corresponding value at the core of the crystal [1,2] and, therefore, high field contributions corresponding to n=0 and 1 can be assumed to be free from this correction.

A simple probabilistic calculation using a binomial distribution for binary $Fe_{100-x}Nb_x$ alloy supplies a probability, *P(n)*, to find a certain number n of Nb atoms as NN or NNN among the 14 atoms forming the two first shells of the probe Fe.

Journal of Alloys and Compounds, 610 (2014) 92-99
http://dx.doi.org/10.1016/j.jallcom.2014.04.195

$$P(n)=\frac{14!}{(14-n)!n!}C(Fe)^{14-n}\,C(Nb)^{n} \tag{2}$$

where *C(Fe)* and *C(Nb)* are the concentration of Fe and Nb, respectively, in the two first shells. The probe region is actually formed by 15 atoms, one of them is mandatorily Fe (the probe atom at the center) and the concentrations *C(Fe)* and *C(Nb)* do not coincide with those of the whole system $C(Fe)^{W}$ and $C(Nb)^{W}$ but they are related as:

$$C(Fe)=\frac{15C(Fe)^{W}-1}{14} \tag{3}$$

$$C(Nb)=\frac{15C(Nb)^{W}}{14} \tag{4}$$

We can estimate *C(Nb)* from the ratio between contributions at 33 T (n=0) and 30 T (n=1), which are those less affected by artifacts or interface region. Only the peak centered at *HF*=27 T could affect, by overlapping, the area of the contributions considered in the following discussion (see Fig. 5). Therefore, if we calculate the ratio between probabilities corresponding to n=1 and n=0 we obtain:

$$\frac{P(1)}{P(0)}=\frac{14\left[1-C(Nb)\right]^{13}C(Nb)}{\left[1-C(Nb)\right]^{14}} \tag{5}$$

From Eq. (4) and Eq. (5), $C(Nb)^{W}$ can be obtained as:

$$C(Nb)^{W}=\frac{14}{15}\frac{\frac{P(1)}{P(0)}}{\left[14+\frac{P(1)}{P(0)}\right]} \tag{6}$$

The values of $C(Nb)^{W}$ obtained are shown in figure 9 along with the values obtained from the lattice parameter evolution using Vegard law and considering a=2.8665 and 3.3002 Å

for pure bcc Fe and Nb, respectively. Taking into account that Vegard law is just a rough estimation, both plots are in good agreement and indicate a fast tendency to saturation of Nb solution in bcc-Fe after 6 h of milling. The saturation value, 3.6±0.5 at. % Nb, is below the nominal one, 5.56 at. % Nb, indicating a slight preferential partitioning of Nb atoms to the boundaries between the crystallites. Figure 9 also shows the resulting values for the B-containing alloys using the same approach (i.e. neglecting the effect of B in the nanocrystals), which leads to almost the same value 4.0±0.4 at. % Nb.

The equilibrium phase diagram shows that solubility of B in bcc Fe is practically null. However, Ray and Hasegawa [25] obtained supersaturated bcc Fe(B) solutions by rapid quenching and they found B atomic impurities in bcc Fe to be preferentially substitutional with three B atoms per two Fe atoms substituted in the lattice. Therefore, lattice parameter decreases as B increases in the alloy with a rate of $\sim -10^{-3}$ Å/at.% B [25]. This small effect, in comparison with that of Nb, prevents any identification of the effect of B in the bcc phase using Vegard law. However, the effect of one B atom as NN of an Fe atom yields a decrease of ~2.7 T in the *HF* of this Fe atom [39]. Although results neglecting B inside crystallites (figure 9) seems an adequate approximation, B must affect the position of the Gaussian functions used to describe the n=0 and n=1 environments. Taking into account an average effect of boron in the Fe environments, a new fitting of the *HFDs* was performed without imposing any value for the centers of the Gaussian functions. In this case, the high field peak observed in experimental *HFDs* was fitted using two Gaussian functions centered between ~34 and ~29 T. The average hyperfine field of these two contributions, $\langle HF(0,1) \rangle$, is shown in figure 10 for both alloys. A 1 T lower value is reached for the B-containing alloy with respect to the B-free alloy, which could be interpreted as the effect of extra impurities in the neighborhood of Fe (i.e. B atoms). As *HF* decreases 0.29 T/at. % B in α-Fe [39], the boron concentration needed to achieve $\langle \Delta HF \rangle$=-1 T is $C(B)$~3.4 at. %, much lower than the nominal composition (10 at.% B). This is in agreement with the presence of boron inclusions as shown in the BSE images and previously found in other Fe-Nb-B alloys with an almost pure boron composition [30].

Journal of Alloys and Compounds, 610 (2014) 92-99
http://dx.doi.org/10.1016/j.jallcom.2014.04.195

4.2 Effect of microstructure

Although differences between high field contributions for both alloys are subtle, a clear difference is observed in the total average hyperfine field, <*HF*>, between the B-containing alloy and the B-free one (figure 6b). Whereas <*HF*> of the B-free alloy initially decreases to remain almost constant after 3.5 h milling, a continuous decrease is observed for the B-containing alloy. This continuous decrease is more pronounced than that observed for <*HF(0,1)*> as the presence of boron is not the only possible cause of it once the complete *HFD* is considered. In fact, as shown in figure 2, the main structural difference between the B-containing and the B-free alloys is the smaller crystal size achieved for the B-containing alloy. The interface region is related to the ratio between the surface and the volume of crystals and, therefore, the amount of interface region, X_{Int}, must be proportional to 1/*D*. On the other hand, the total average value of *HF* can be separated in the core contribution, $\langle HF_{core} \rangle$, and the interface contribution, $\langle HF_{Int} \rangle$, as follows:

$$\langle HF \rangle = (1 - X_{Int}) \langle HF_{core} \rangle + X_{Int} \langle HF_{Int} \rangle = \frac{k}{D} \left(\langle HF_{Int} \rangle - \langle HF_{core} \rangle \right) + \langle HF_{core} \rangle \qquad (7)$$

where *k* is a geometrical constant. For a spherical shell $k=6t$, being t~1 nm the thickness of the interface for bcc crystals [1] Figure 11b shows the plot of <*HF*> versus 1/*D* for both studied alloys. A good linear relationship is found. Fitting the data of the B-containing alloy to a straight line leads to a value of $\langle HF_{core} \rangle = 31.2 \pm 0.2$ T. The value of $\langle HF_{core} \rangle$ can be estimated neglecting B content as:

$$\langle HF_{core} \rangle = 33 - \sum_{n=1}^{14} (\Delta HF)_n \cdot M_n \cdot {C_{Nb}}^n (1 - C_{Nb})^{14-n} \qquad (8)$$

where $(\Delta HF)_n = -3.0n$ T for n=1 and 2 (as described above, after averaging the results of ref. [35]); for n=3 and 4 they have been taken from the fitting results of the complete *HFDs* (21.5 and 14.5 T, respectively) and for n>4, $(\Delta HF)_n$=-33 T (paramagnetic contribution). In any case, the effect of high values of *n* are negligible as the compositions considered should have a small

Journal of Alloys and Compounds, 610 (2014) 92-99
http://dx.doi.org/10.1016/j.jallcom.2014.04.195

content of Nb. Graphical solution of equation $<HF_{core}>$=31.2 T yields C_{Nb}^{W}=3.9±0.4 at. % Nb, in very good agreement with our previous result. However, it is worth mentioning that previous analysis allowed us to determine the fast increase in Nb content at the early stages of milling, whereas this new analysis is blind to that effect as the change of 1/*D* at the early stages is very abrupt and completely jeopardizes the initial change in Nb content inside the nanocrystals. The concentration of B inside the nanocrystals is low enough to be negligible and B atoms might be preferentially located forming inclusions and at the grain boundaries.

Finally, although the causes affecting *HF* are both compositional and structural, the linear relationship between this magnitude and the spontaneous specific magnetization, σ_S, is preserved. This linearity is derived from the relationship between *HF* and the magnetic moment [22].

$$HF(i) = b\mu(i) + c\sum_{j}\mu(j) \tag{9}$$

where *i* corresponds to the probe atom (i.e. Fe) and the summatory is extended to each *j* neighbor atom. Using the results from Kobayashi et al. [40], there is an antiparallel induced magnetic moment in Nb atoms in bcc Fe(Nb) that leads to a decrease of the average magnetic moment of $\Delta\mu(TM)$=-0.035 μ_B/at.% Nb. Moreover, from Ray and Hasegawa [25] the average magnetic moment reduces -0.01 μ_B/at. % B. Combining results from Mössbauer [35] and magnetic moment calculations [40] for bcc Fe(Nb), a slope of $\Delta HF/\Delta\mu(TM)$=12±1 T/μ_B and a positive intercept of 6±3 T are obtained. In our case, the slope and intercept for the B-containing alloy are 21.7±1.0 T/μ_B and -10.4±1.7 T, respectively (Figure 11a). Concerning the slope and the intercept, the difference between the values estimated from the literature data and those experimentally obtained in this study can be related to several effects, including compositional changes during milling. In fact, Dubiel [41] has empirically studied the linearity between *HF* and μ concluding that it is not unique but characteristic of each type of alloy or compounds.

In any case, due to the experimentally observed linear dependence of <*HF*> with $\mu(TM)$, a linear dependence with $1/D$ is also expected for $\mu(TM)$, as shown in figure 11c. Linear fitting of the data of the B-free and the B-containing alloys leads to intercept values corresponding to the core value of 1.977±0.014 μ_B and 1.914±0.008 μ_B, respectively. Taking into account that B content in bcc-Fe leads to a decrease of the magnetic moment of -0.01 μ_B per at. % B [25], the difference between the B-free and the B-containing alloys could be due to 6.3±2.2 at. % B inside the nanocrystals, which is in agreement with the results presented above.

Conclusions

Combining results obtained from Mössbauer spectroscopy, X-ray diffraction and magnetic measurements, it has been possible to elucidate the composition of tiny nanocrystals developed during mechanical alloying without requiring the use of nanoscopic techniques, which are more expensive and less available. The ideas used in this paper can be easily extended to other compositions containing Fe, or other nuclei suitable for Mössbauer spectroscopy and, in general, for nuclear magnetic resonance spectroscopies.

Analysis of the ratio between the two highest field contributions to Mössbauer spectra, assumed to be free of interface effects, to the hyperfine field distribution allowed us to follow the progressive enrichment in Nb content of the bcc Fe-based nanocrystals as milling time progresses. This Nb content rapidly increases to a saturation value which is about 90 % of the nominal one, implying a slight enrichment in Nb of the intergranular regions. Comparison between the B-containing and the B-free alloys yields a maximum boron content inside the nanocrystals of ~5 at. % (50 % the nominal value). The excess of boron can be found as crystalline boron inclusions and probably also in B and Nb enriched intergranular region.

A clear linear dependence of the average hyperfine field and the magnetic moment with the inverse of the crystal size is observed, which can be explained by an increase of the fraction

of atoms at interface region. For the studied alloy containing B, a smaller crystal size is observed which could be due to the extra milling effect produced by the presence of hard boron inclusions embedded in the powder particles.

Acknowledgements

This work was supported by the Spanish Ministry of Science and Innovation and EU FEDER (Project MAT 2010-20537), the PAI of the Regional Government of Andalucía (Project P10-FQM-6462).

Journal of Alloys and Compounds, 610 (2014) 92-99
http://dx.doi.org/10.1016/j.jallcom.2014.04.195

Figure 1. XRD patterns of the two studied alloys as a function of the milling time (Color online).

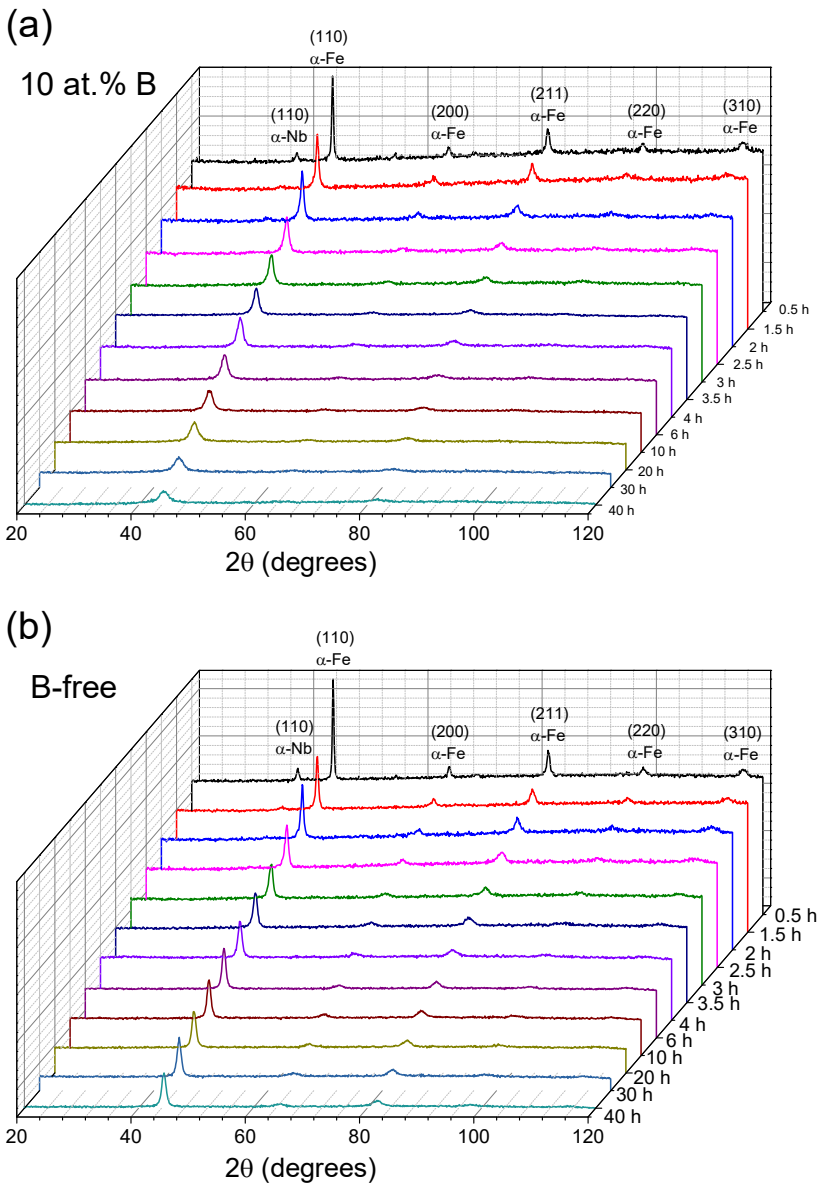

Journal of Alloys and Compounds, 610 (2014) 92-99
http://dx.doi.org/10.1016/j.jallcom.2014.04.195

Figure 2. Evolution of microstrains, crystal size and lattice parameter of the bcc Fe(Nb,B) phase as a function of the milling time. Errors in ε and D are smaller than the symbol size (Color online).

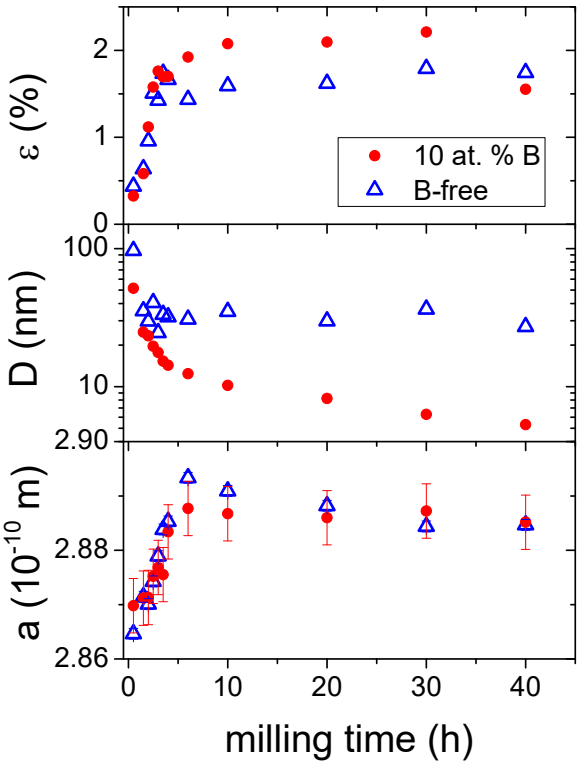

Journal of Alloys and Compounds, 610 (2014) 92-99
http://dx.doi.org/10.1016/j.jallcom.2014.04.195

Figure 3. Back scattered electron images after 0.5 h. b and c show an enlarged view of the area marked in a and b, respectively (Color online).

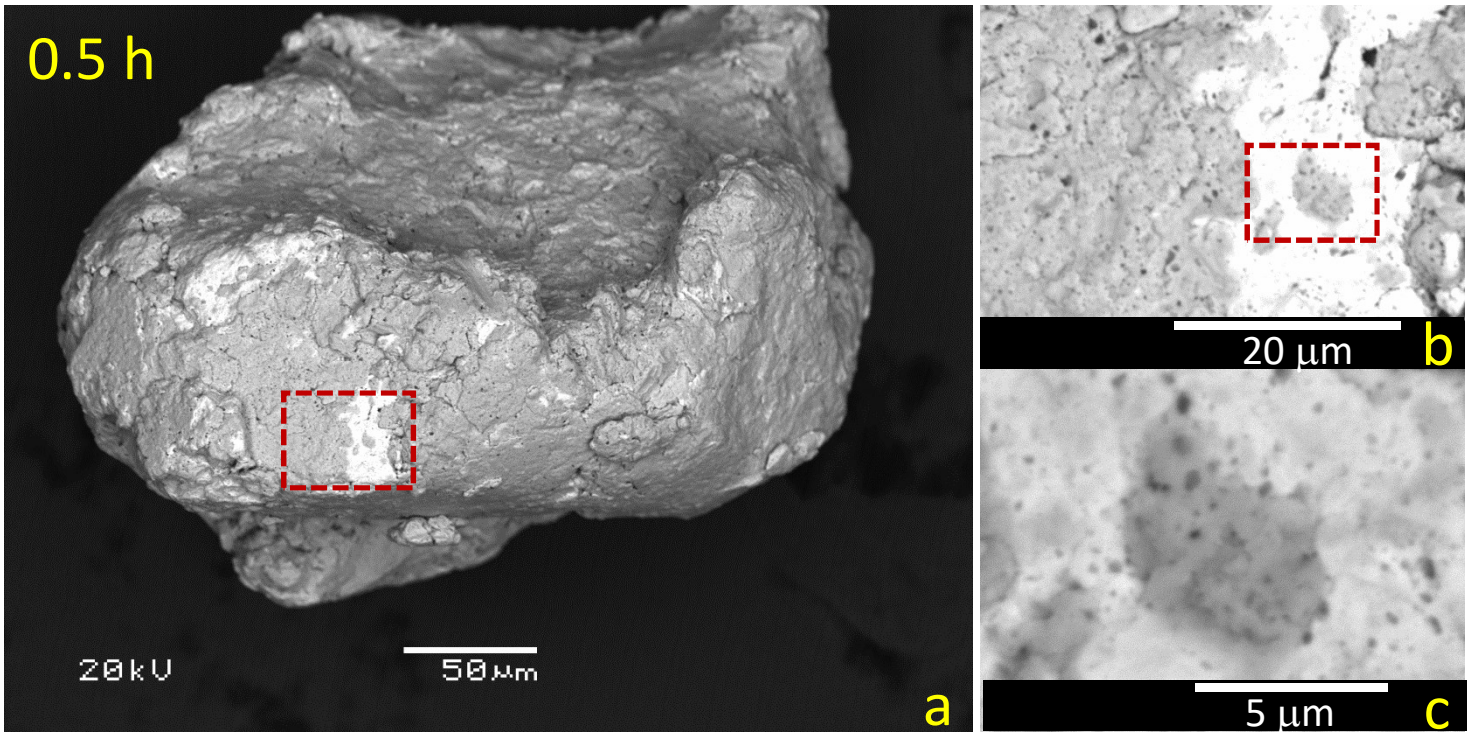

Journal of Alloys and Compounds, 610 (2014) 92-99
http://dx.doi.org/10.1016/j.jallcom.2014.04.195

Figure 4. Mössbauer spectra. Symbols correspond to experimental data and lines to the total fitting as well as to the two *HFD* used (Color online).

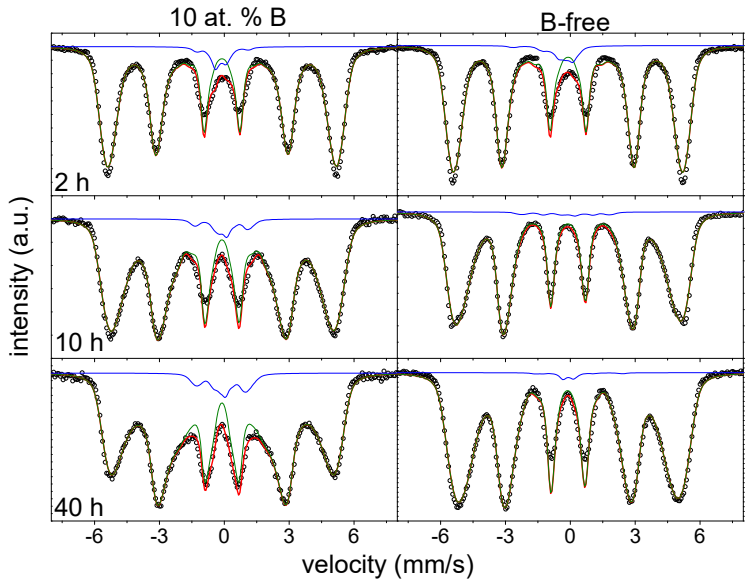

Journal of Alloys and Compounds, 610 (2014) 92-99
http://dx.doi.org/10.1016/j.jallcom.2014.04.195

Figure 5. Probability distribution of the *HF* contributions. Symbols correspond to the data obtained from fitting shown in Fig. 4, color lines represent the Gaussian functions used to fit the high *HF* contributions and the black line corresponds to the total fit using these Gaussian peaks (Color online).

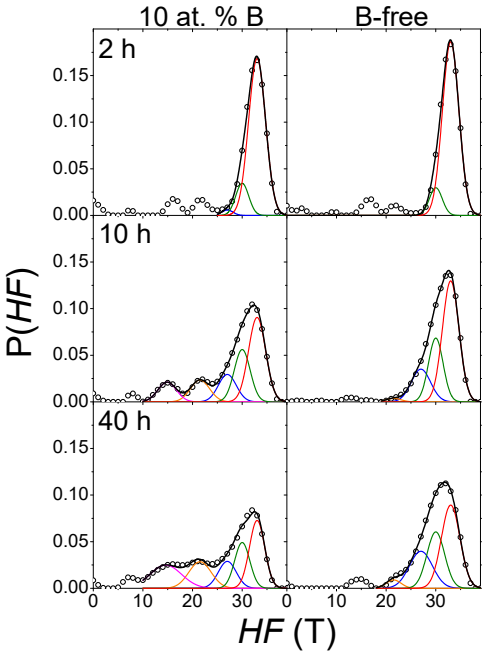

Journal of Alloys and Compounds, 610 (2014) 92-99
http://dx.doi.org/10.1016/j.jallcom.2014.04.195

Figure 6. Mössbauer parameters and magnetization results as a function of milling time: (a) fraction of contributions at *HF*<5 T; (b) average hyperfine field (<*HF*>) (errors smaller than symbol size); (c) average isomer shift (<*IS*>); and (d) spontaneous specific magnetization (errors smaller than the symbol size). Lines are a guide to the eye.

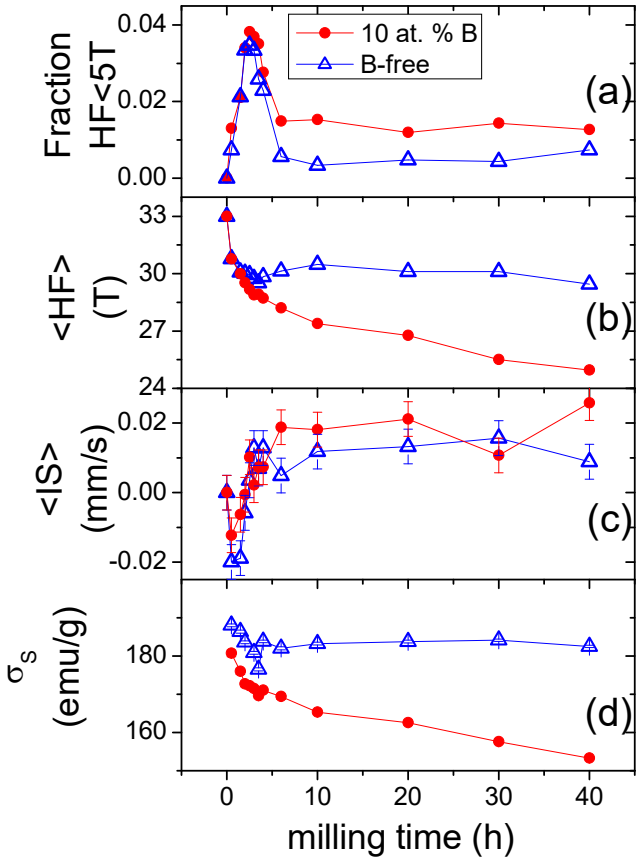

Journal of Alloys and Compounds, 610 (2014) 92-99
http://dx.doi.org/10.1016/j.jallcom.2014.04.195

Figure 7. Magnetization curves at room temperature for both studied alloys.

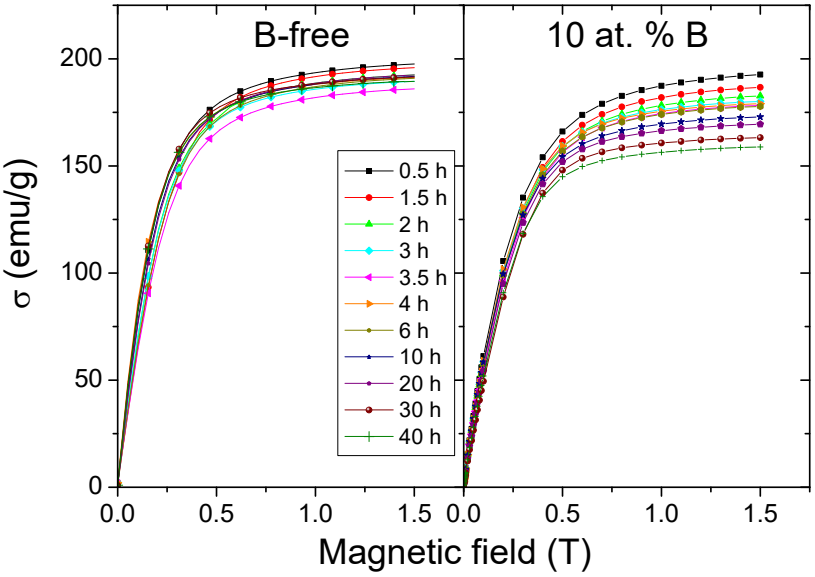

Journal of Alloys and Compounds, 610 (2014) 92-99
http://dx.doi.org/10.1016/j.jallcom.2014.04.195

Figure 8. Simple cartoon in two dimensions illustrating the evolution of Nb crystals at the early stages of milling (Color online).

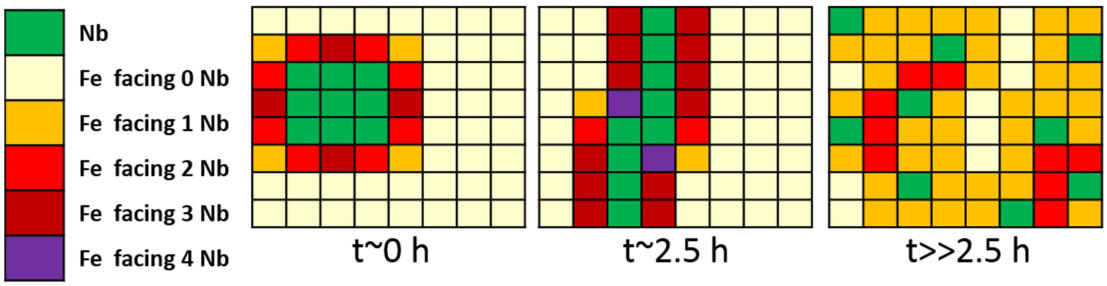

Journal of Alloys and Compounds, 610 (2014) 92-99
http://dx.doi.org/10.1016/j.jallcom.2014.04.195

Figure 9. Content of Nb inside the nanocrystals from Mössbauer results and Vegard's law.

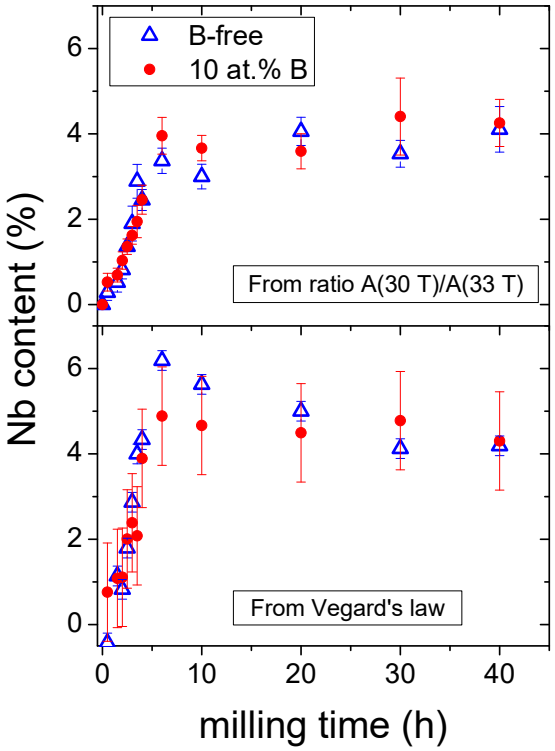

Journal of Alloys and Compounds, 610 (2014) 92-99
http://dx.doi.org/10.1016/j.jallcom.2014.04.195

Figure 10. Average hyperfine field of the two highest contributions used to fit *HFD*s. Errors are smaller than the symbol size.

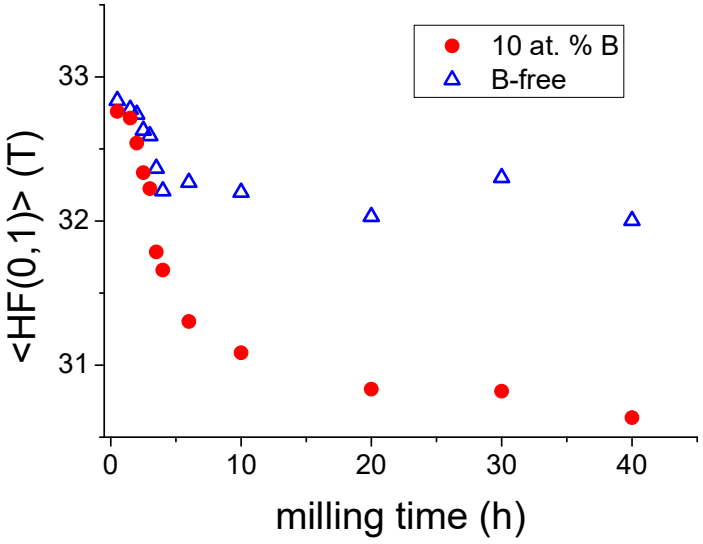

Journal of Alloys and Compounds, 610 (2014) 92-99
http://dx.doi.org/10.1016/j.jallcom.2014.04.195

Figure 11. (a) Average hyperfine field as a function of the magnetic moment per transition element. (b) Average hyperfine field as a function of the inverse of the crystal size. (c) Magnetic moment as a function of the inverse of the crystal size. Dotted lines correspond to linear fitting to the data.

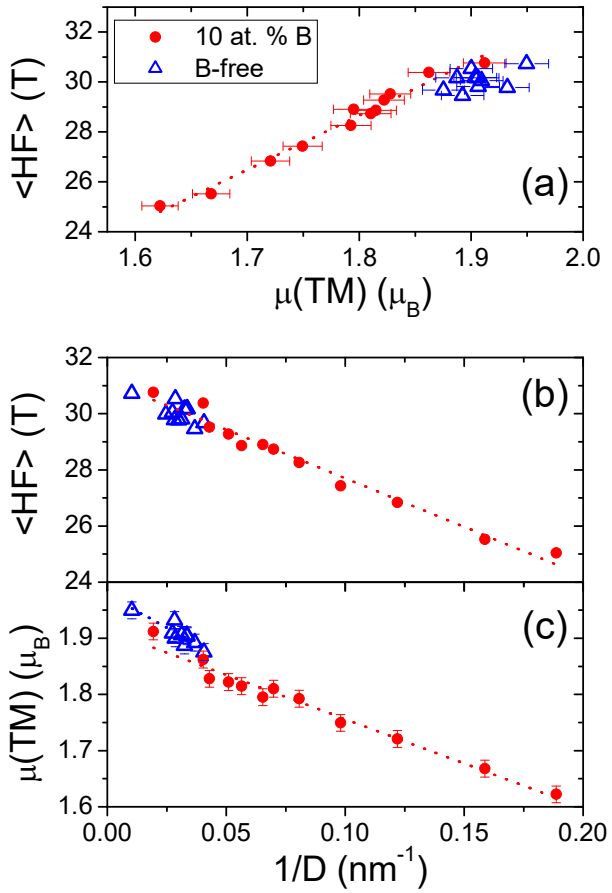

Journal of Alloys and Compounds, 610 (2014) 92-99
http://dx.doi.org/10.1016/j.jallcom.2014.04.195

References

[1] B. Fultz, H.N. Frase, Hyperfine Interactions 130 (2000) 81-108.
[2] J. M. Greneche, Hyperfine Interactions 110 (1997) 81-91.
[3] M. A. Chuev, A. M. Afanasev, J. Hesse, O. Hupe, New trends in Mössbauer Spectroscopy focused on nanostructured magnetic materials: evaluation, theory and methodology, in Materials Research in Atomic Scale by Mössbauer Spectroscopy, Edited by M. Mashlan, M. Miglierini, P. Schaaf, Kliver Academic Publishers, Dordrecht 2002
[4] J. Balogh, L. Bujdosó, D. Kaptás, T. Kemény, I. Vincze, S. Szabó, D. L. Beke, Phys. Rev. B 61 (2000) 4109-4116
[5] T. G. Woodcock, Y. Zhang, G. Hrkac, G. Ciuta, N. M. Dempsey, T. Schrefl, O. Gutfleisch, D. Givord, Scripta Mater. 67 (2012) 536-541
[6] B. Balamurugan, D. J. Sellmyer, G. C. Hadjipanayis, R. Skomski, Scripta Mater. 67 (2012) 542-547
[7] M. Willard, M. Daniil, K. E. Kniping, Scripta Mater. 67 (2012) 554-559
[8] C. Suryanarayana, Prog. Mater. Sci. 46 (2001) 1-184
[9] J. Sort, S. Suriñach, J. S. Muñoz, M. D. Baró, J. Nogues, G. Chouteau, V. Skumryev, G. C. Hadjupanayis, Phys. Rev. B 65 (2002) 174420
[10] N.G. Akdogan, G. C. Hadjipanayis, D. J. Sellmyer, Nanotechnology 21 (2010) 295705
[11] W. F. li, H. Sepehri-Amin, L. Y. Zheng, B.Z. Cui, A. M. Gabay, K. hono, W. J. Huang, C. Ni, G. C. Hadjipanayis, Acta Mater 60 (2012) 6685-6691
[12] V. Velasco, A. Hernando, P. Crespo, J. Magn. Magn. Mat. 343 (2013) 228-233
[13] J. S. Blázquez, J. J. Ipus, S. Lozano-Pérez, A. Conde, JOM 65 (2013) 870-882
[14] J. S. Benjamin, T. E. Volin, Metal. Trans. 5 (1974) 1929-34
[15] Y. Jiraskova Y, J. Bursik, I. Turek, J. Supercond. Nov. Mag. 26 (2013) 1717-21.
[16] E. P. Yelsukov, A. Maratkanova, S. F. Lomayeva, G. N. Konygin, O. M. Nemtsova, A. I. Ul'yanov A. A. Chulkina, J. All. Compd. 407 (2006) 98-105.
[17] S. F. Lomayeva, A. N. Maratkanova, Intermetallics. 17 (2009) 714-21
[18] B. Pandey, M. A. Rao, H. C. Verma, S. Bhargava, J. Phys. Cond. Matter, 17 (2005) 7981-93
[19] J. J. Ipus, J. S. Blázquez, S. Lozano-Pérez, A. Conde, Phil. Mag. 89 (2009) 1415-1423
[20] I. Kaban, P. Jovari, A. Waske, M. Stoica, J. Bednarcik, B. Beuneu, N. Mattern, J. Eckert, J. All. Compd. 586 (2014) S189-93
[21] P. Gütlich, E. Bill, A. X. Trautwein, Mössbauer Spectroscopy and Transition Metal Chemistry. Fundamentals and Applications, Springer-Verlag, Heidelberg 2011
[22] Y. D. Zhang, J. I. Budnick, J. C. Ford, W. A. Hines, J. Magn. Magn. Mater. 100 (1991) 13-37
[23] G.S. Pawley, J. Appl. Crystallogr. 14 (1981) 357
[24] R. A. Brand, J. Lauer, D. M. Herlach, J. Phys. F: Met. Phys. 13 (1983) 675
[25] R. Ray, R. Hasegawa, Solid State Comm. 27 (1978) 471-474
[26] J. J. Ipus, J. S. Blázquez, V. Franco, A. Conde, Intermetallics 16 (2008) 1073-1082
[27] J. J. Ipus, J. S. Blázquez, V. Franco, S. Lozano-Pérez, A. Conde, J. All. Compd. 553 (2013) 119
[28] K. Kanaya, S. Okayama, J. Phys. D: Appl. Phys. 5 (1972) 43-58
[29] M. Dapor, Phys. Rev. B 46 (1992) 618-625
[30] J. J. Ipus, J. S. Blázquez, V. Franco, A. Conde, M. Krasnowski, T. Kulik, S. Lozano-Pérez, J. Appl. Phys. 107 (201) 073901
[31] M. Krasnowski, T. Kulik, Intermetallics 28 (2012) 120-127
[32] M. Krasnowski, A. Antolak-Dudka, T. Kulik, Intermetallics 19 (2011) 1243-1249
[33] J. Balogh, L. Bujdosó, D. Kaptás, I. Dézsi, A. Nakanishi, Phys. Rev. B 85 (2012) 195429
[34] R. Ingalls, H. G. Drickamer, G. De Pasquali, Phys. Rev. 155 (1967) 165-170.
[35] A. Blachowski, K. Ruebenbeuer, J. Zukrowski, Phys. Stat. Sol. B 242 (2005) 3201-3208.
[36] D. S. Schmool, E. Araujo, M. M. Amado, M. Alegria Feio, D. Martín Rodríguez, J. S. Garitaonandia, F. Plazaola, J. Magn. Magn. Mater. 272-276 (2004) 1342-1344
[37] M. B. Stearns. Phys Rev 129 (1963) 1136-1144
[38] J. M. Borrego, J. S. Blázquez, C. F. Conde, A. Conde, S. Roth, Intermetallics 15 (2007) 193-200
[39] F. H. Sánchez, M. B. Fernández van Raap, J. I. Budnick, Phys. Rev. B 46 (1992) 13881-13887
[40] M. Kobayashi, T. Kai, N. Takano, Y. Ohashi, K. Shiiki, J. Magn. Magn. Mater. 166 (1997) 329-333.
[41] S. M. Dubiel, J. All. Compd. 488 (2009) 18-22.